HHS Public Access

Author manuscript

Magn Reson Med. Author manuscript; available in PMC 2016 December 01.

Published in final edited form as:

Magn Reson Med. 2015 December ; 74(6): 1750–1757. doi:10.1002/mrm.25566.

Engineering an effective Mn-binding MRI reporter protein by subcellular targeting

Benjamin B. Bartelle[1,3], **Miyeko D. Mana**[1,4], **Giselle A. Suero-Abreu**[1], **Joe J. Rodriguez**[1], and **Daniel H. Turnbull**[1,2,*]

[1]Skirball Institute of Biomolecular Medicine, New York University School of Medicine, New York, New York, USA

[2]Departments of Radiology and Pathology, New York University School of Medicine, New York, NY, USA

[3]Department of Biological Engineering, Massachusetts Institute of Technology, Cambridge, MA, USA

[4]Koch Institute of Integrative Cancer Research, Massachusetts Institute of Technology, Cambridge, MA, USA

Abstract

Purpose—Manganese (Mn) is an effective contrast agent and biologically active metal, which has been widely utilized for Mn-enhanced MRI (MEMRI). The purpose of this study was to develop and test a Mn binding protein for use as an genetic reporter for MEMRI.

Methods—The bacterial Mn-binding protein, MntR was identified as a candidate reporter protein. MntR was engineered for expression in mammalian cells, and targeted to different subcellular organelles, including the Golgi Apparatus where cellular Mn is enriched. Transfected HEK293 cells and B16 melanoma cells were tested in vitro and in vivo, using immunocytochemistry and MR imaging and relaxometry.

Results—Subcellular targeting of MntR to the cytosol, endoplasmic reticulum and Golgi apparatus was verified with immunocytochemistry. After targeting to the Golgi, MntR expression produced robust R1 changes and T1 contrast in cells, in vitro and in vivo. Co-expression with the divalent metal transporter DMT1, a previously described Mn-based reporter, further enhanced contrast in B16 cells in culture, but in the in vivo B16 tumor model tested was not significantly better than MntR alone.

Conclusion—This second-generation reporter system both expands the capabilities of genetically-encoded reporters for imaging with MEMRI and provides important insights into the mechanisms of Mn biology which create endogenous MEMRI contrast.

Keywords

manganese (Mn); Mn-enhanced MRI (MEMRI); molecular imaging; MntR; DMT1

*Correspondence to: Daniel H. Turnbull, Ph.D., Skirball Institute of Biomolecular Medicine, New York University School of Medicine, 540 First Avenue, New York, NY USA 10016, daniel.turnbull@med.nyu.edu.

INTRODUCTION

Manganese (Mn) has been used extensively as a contrast agent in MRI, with an expanding range of applications (1). In most cases, Mn-enhanced MRI (MEMRI) has relied on endogenous mechanisms of cellular Mn uptake and retention to generate tissue-specific contrast in vivo. Previous reports have shown the utility of MEMRI for imaging neural activity, via uptake of Mn through voltage-gated calcium channels (2,3), and for in vivo tract tracing, via microtubule-mediated transport of Mn along axons and across synapses (4,5). We recently presented a genetic method to engineer Mn uptake in cells through the expression of the Divalent Metal Transporter, DMT1 (6). Currently most MEMRI methods, including the use of DMT1 as a reporter protein, focus on delivery and uptake of Mn to cells and tissues, relying on endogenous methods of Mn retention and transport in the cells of interest. The details of cellular Mn trafficking and metabolism after uptake are not well understood, and only a few mechanisms have been elucidated (7–9). In this study, we explored retention of Mn as a platform to further engineer contrast for a MEMRI reporter system, and to better understand the underlying mechanisms of subcellular Mn trafficking.

Given the past successes of MEMRI, retaining Mn within cells of interest with a Mn-binding protein is a logical strategy for a genetically-encoded MRI contrast agent. Chelates of paramagnetic metals, usually gadolinium, are the most common contrast agents for clinical MRI (10) and serve as a model for engineering a biological equivalent. Attaching gadolinium or other paramagnetic atoms to a chemical chelator reduces the toxicity of a heavy metal ion, can improve relaxivity, and provides a scaffold for engineering functionality for imaging studies. In metal chelate-based T1-shortening contrast agents, a critical feature is the exposure of the paramagnetic metal to the surrounding solvent / spin lattice, allowing the ready exchange of water protons. Sequestration of the paramagnetic metal demonstrably reduces proton exchange to quench T1 effects, a phenomenon that has been used to great advantage for designing MRI sensor molecules and enzymatically activated contrast agents (11,12)

Biological chelators of metal ions are abundant as structural or reactive elements in proteins. Though less common than calcium (Ca) or iron (Fe), Mn is an essential cofactor for many enzymes such as Arginase I (13), Prolidase (14), and Superoxide Dismutase (15). Structural analysis reveals that Mn binding motifs are often deep within these proteins, away from solvent. Having a sequestered metal chelate is not unusual for an enzyme reaction center, but does not allow for ready exchange of water and would minimize the ability of Mn to transfer energy to the spin lattice and lower the T1 effect. Other proteins such as glycosyltransferases bind Mn in a much more open conformation, but these enzymes have a poor selectivity for the metal (16,17). The metalloregulatory protein MntR, originally identified in the bacteria *B. subtilis*, has high selectivity to Mn while leaving the chelated metal exposed to the spin lattice (18,19). Like all cells, *B. subtilis* requires Mn as a trace element and cofactor, while excessive Mn can be toxic to cells as it can readily interact with iron (Fe) or calcium (Ca) binding sites. To maintain homeostatic levels of Mn within the cell, the bacteria must have a means of sensing Mn, and MntR serves this role (3). Mn binding in MntR results in a protein conformation, which binds DNA and acts as a repressor of metal transport proteins, phylogenetically related to DMT1 (20,21). The 17kD protein

binds Mn in two adjacent sites with affinities (K_d) ranging from 0.2–13μM (19). Moreover, MntR binds Mn with high specificity; physiological levels of Fe or Ca are not competitive for binding. Only cadmium (Cd), which is extremely rare in vivo, has a similar affinity for the protein.

Simply finding a chelator of Mn is clearly not sufficient, as a previous chemical sensor with picomolar affinity for Mn has failed to detect Mn under basal physiological conditions (22). This points to broader considerations of Mn biology occurring at the subcellular level. Subcellular imaging studies have shown, at a basal state, that Mn is sparse in the cytoplasm and localized in specific organelles, including the nucleus, mitochondrion, and the secretory pathway (23). Early studies with reconstituted organelles demonstrated that the Sarcoplasmic/Endoplasmic Reticulum Ca specific (SERCA) pumps could actively transport Mn to the endoplasmic reticulum (ER), albeit at low efficiency, and only at concentrations above 200μM (24). A growing body of more recent work now suggests that Mn is actively accumulated elsewhere under in vivo conditions. Correlative imaging with X-ray fluorescence and immunofluorescence suggests it is the Golgi apparatus (GA), adjacent to the ER, that contains the highest levels of Mn, even when cells are supplemented with the metal at levels equivalent to MEMRI doses (25). This is consistent with the observation that glycosyltransferases, which use Mn as a cofactor despite having a low affinity for the metal, are resident in the GA (8,26). Having a high local concentration of Mn is absolutely necessary for the proper function of these enzymes. Further support for the hypothesis that the GA functions as an important storage organelle for Mn has come with the characterization of a Mn specific P-type pump, SPCA1, and biochemical assays for GA specific Mn (27,9).

Based on the above criteria, we sought to develop a chelation based contrast agent that would bind Mn in a solvent exposed fashion and be localized within the GA where Mn concentrations are expected to be high. In this study we used these specifications as the design basis for a new type of reporter protein based on the chelation of Mn. We began by studying the atomic structures of known Mn binding proteins and identified the bacterial Mn sensor MntR as an excellent candidate based on it's specificity for Mn and solvent exposed Mn binding motif (19). We then targeted the protein to the GA by making a fusion to one of its resident proteins, Cab45. The result is a biological contrast agent that provides robust Mn based signal in cells from hours to days, offering an iterative improvement upon and complement to DMT1.

METHODS

Bacterial MntR expression

MntR in an inducible pET17b vector, previously used in structural studies (NCBI protein databank entry PDB:1ON2), was transformed into chemically competent BL21 bacterial cells (18). Bacterial cultures (2mL) were grown overnight in LB media under ampicillin selection and used to inoculate 50mL cultures of 2XYT media. Cultures were grown to an optical density of 1.0 and Isopropyl β-D-1-thiogalactopyranoside (IPTG) was added to 1mM to induce MntR expression. Cultures were grown for an additional 2 hours, after which 1mL aliquots were removed from each culture and centrifuged into 1.5mL tubes. Bacteria were

washed in 1mL PBS and fixed for 15 minutes in cold PFA. The bacterial pellets were then transferred to NMR tubes for MRI and relaxometry.

Constructs and Stable Cell lines

A mammalian expression optimized version of the MntR gene was synthesized by BioBasic Inc. The original sequence was run through an algorithm that reassigned the codons most compatible for mouse tRNAs and for the most stable mRNA. A Myc tag was introduced to the C-terminus of the protein. The reengineered gene was then put into the pIRES-eGFP expression vector and pCDNA3.1 for transient transfection, and into a retroviral construct to generate stable cell lines. Retroviral MntR stable cell lines were generated using previously described methods (6), using a CMV promoter driving coexpression (via an IRES) of both MntR and eGFP. An ER targeted version of MntR was generated by fusion to known targeting signals. The N-terminal signal sequence and C-terminal KDEL ER retention sequence were derived from the ER chaperone protein BiP and fused to MntR using synthetic PCR with long oligonucleotides of the targeting sequences. A Golgi targeted version of MntR was generated by fusion to the full length Golgi native protein Cab45 and its shortest isoform by alternative splicing. The whole mCherry-Cab45 gene was synthesized and included convenient sites for fusion of the Cab45 element into MntR (^{Cab45}MntR) or MntR^{KDEL} (^{Cab45}MntR^{KDEL}, denoted as MntR*) using restriction site cloning. For in vivo expression of both MntR* and DMT1, the two proteins cloned into a single fusion transcript with a T2A peptide linker, allowing for multicistronic translation from a single open reading frame (28). GFP was still expressed via an IRES to avoid interactions with the C-terminal KDEL with the final construct consisting of DMT1^{T2A}MntR*-IRES-eGFP.

Transfections of all MntR chimeras with IRES-eGFP and the combined DMT1^{T2A}MntR*-IRES-eGFP construct were grown for 7 days in HEK293T cells and sorted using flow cytometry for cells with $>10^3$ log units of eGFP fluorescence. For stable B16 melanoma cells both constructs were placed under neomycin selection for 7 days prior to sorting for cells with $>10^{2.5}$ log units of eGFP signal.

Cell Staining

All MntR chimeras were transiently transfected using a chemical transfection reagent (Mirus Bio) into HEK293T growing on glass slides. Cells were fixed with PFA and immunocytochemistry was conducted using and anti-Myc antibody for the integrated Myc tag into MntR (1:500 Abcam), anti-Calnexin as an ER-marker (1:500 Abcam) and anti-58K as a GA marker (1:500 Abcam). Fluorescent Red, Green, and Blue secondary antibodies were used to co-label all markers in each cell. Immunolabeled cells were imaged using an epifluorescence microscope (Leica MZ16F).

MRI of Cell Lines

Relaxometry was performed as previously described (6). Briefly, cells were supplemented with $MnCl_2$ (100–300μM) for 1h, washed with PBS, trypsinized and gently pelleted for imaging. Cell pellets were imaged on a 7T Bruker Biospec system, using a T1-weighted 2D multislice Gradient Echo (2DGE) sequence (echo time, TE = 3.1ms; repetition time, TR = 100ms; flip angle, FA = 45°) and a 2D multi- slice Spin Echo (2DSE) saturation recovery

sequence (TE = 11ms; TR = 190ms, 500ms, 900ms, 1.5s, 3s), both with in-plane resolution of 100 × 100μm^2 and 500μm slice thickness. 2DSE images with increasing TR values were used to calculate a T1 map using the MRI Analysis Calculator Plugin for ImageJ. Data were plotted as R1(=1/*T*1) (mean standard deviation).

In Vivo MRI of B16 Melanoma Models

All mice were maintained under protocols approved by the Institutional Animal Care and Use Committee at NYU School of Medicine. Melanomas were generated by injecting 10^6 B16 melanoma cells subcutaneously into both flanks of C57Bl/6 adult mice and grown in vivo for 9–10 days before imaging.

Mice were imaged on a 7T Bruker Avance II Biospec system (Paravision 4), using a T1-weighted 2DGE sequence (TE/TR = 3.1/50ms; FA = 45°; in-plane resolution = 100 × 100μm^2; slice thickness = 500μm) Mice with tumors were given an IP injection of an aqueous solution of $MnCl_2$ (80mg/kg) and imaged 3h and 6h post injection. All mice were anaesthetized with ~1.5% isofluorane in air during MRI and maintained at 37°C with warm air.

Data analysis was carried out on cross sectional images including both tumors of the dual tumor models. ROI's were selected of whole tumors despite heterogeneity to avoid bias, however, tumors with large hypointense regions, indicative of necrosis, were considered artifacts and excluded from the study.

Statistical Analysis

MRI contrast was computed as:

$$\text{Contrast} = (\text{Test} - \text{Control}) / \text{Control}.$$

The control region in all cases was the contralateral wild-type B16 tumor. Contrast values were expressed as a percentage difference. Significance was determined with a two-tailed Student's t-test ($p < 0.05$), and all variation was expressed as the standard deviation from the mean value.

RESULTS

MntR was identified as a candidate Mn-binding reporter protein for MRI

Initial MRI experiments with MntR were performed using an existing bacterial expression construct (18). Bacterial cells with induced expression of MntR showed a 110% change in R1 compared to naive bacteria, without any additional supplementation of Mn to the media beyond the trace (low μM) levels essential for growth (Figure 1a,d). These data suggested that MntR expression retained Mn in the cell and had potential for use as an MRI reporter in eukaryotic cells. MntR was therefore engineered for expression in mammalian cells and transfected transiently into human embryonic kidney (HEK) cells Figure 1b,c). In contrast to the results in bacterial cells, MntR-expressing (+*MntR*) HEK cells did not demonstrate any significant difference comparing R1 values measured in living HEK control and +*MntR* cells, even when supplemented with additional Mn (Figure 1c,d). Once fixed in PFA and left

for several hours however, visible contrast became apparent in *+MntR* cells compared to control (Figure 1b,d). Since fixation allows Mn ions to relocate and freely diffuse throughout and even out of the Mn-treated cells, these data suggested that some mechanism in living mammalian cells prevented the binding of Mn to MntR, such as active sequestration of Mn away from the cytosol where the ectopically expressed MntR protein was localized.

MntR can be effectively targeted to cellular organelles

Previous reports have demonstrated that cellular Mn is actively transported into the GA by Ca- and Mn-specific ATP2C pumps (9,25). We explored the possible role MntR localization could have by generating chimeras of MntR with other proteins or domains that target the ER and the GA (Figure 2a). The ER targeted MntR was a fusion with an N-terminal signal sequence and a C-terminal KDEL peptide sequence from the ER chaperone protein BiP (29). These domains have been identified as the means of initially translating the protein into the rough ER, via the signal sequence, and returning it there from the cis-Golgi, via the KDEL sequence; they are otherwise not functional components of BiP. To our knowledge there is no known peptide sequence tag that can be used to localize a soluble protein to the interior of the GA. Targeting MntR to the GA was therefore achieved by generating a 60kD fusion to a soluble Golgi resident protein, Cab45 (30). The whole protein sequence was used, as it is unknown what domain retains Cab45 to the GA. Unlike the ER, the GA is a multi-compartment organelle, meaning that any given Golgi protein will not necessarily be ubiquitous throughout every part of the organelle. The ATP2C pumps are less common in the trans-Golgi network (27), making Mn less abundant for the targeted MntR, or the chimera could drift into secretory vesicles and get secreted from the cell. Therefore, a double chimera was also made, using the Cab45-MntR fusion protein together with the KDEL sequence, in an attempt to restrict the protein to the cis-Golgi where the KDEL receptor actively loads proteins with the KDEL sequence into COP1 vesicles for recycling back to the ER (31).

Expression of non-chimerical MntR was cytoplasmic, much like that of untargeted GFP in the cell (Figure 2b). This was expected, as bacteria do not have the same internal organelle structures as eukaryotes and therefore do not have organelle-specific targeting sequences. The BiP chimera ^{SS}MntR^{KDEL} effectively targeted the ER resulting in colocalization with the ER marker, calnexin. The ^{Cab45}MntR fusion localized to the GA as did the ^{Cab45}MntR^{KDEL}, referred to as MntR* (Figure 2b). Immunocytochemistry did not reveal an obvious difference between the distribution of ^{Cab45}MntR and MntR* within the GA, but differences in the relative amounts of tagged protein in sub-Golgi compartments would not be detectable using immunocytochemistry.

Targeting MntR to specific organelles generated differences in T1-relaxation

Each cell line was assayed by supplementing for one hour with 300μM $MnCl_2$ to approximate a typical Mn dose in MEMRI (32). Without Mn-supplementation, no R1 differences were apparent, similar to previous work with the DMT1 reporter (6). Expression of unmodified MntR yielded no significant differences in R1 compared to control HEK cells (Figure 3a). The ER targeted chimera, ^{SS}MntR^{KDEL}, was similarly ineffectual at producing

R1 changes (Figure 3a). The GA targeted chimeras, however, did produce improvements in R1. ^{Cab45}MntR fusion alone gave a small, but significant, 11% gain in R1 over control cells. The largest gains came from the MntR* chimera, creating a 30% increase in R1 compared to control and a significant improvement over ^{Cab45}MntR alone.

In HEK cells, the *+MntR** cell line gave even greater contrast at 300μM than transient transfection (Figure 3b,c), or a 49% increase in R1. Comparison of HEK and *+MntR** cells over varying concentrations of Mn demonstrated the protein's effect on Mn kinetics. At low levels of Mn, the cell lines were not significantly different in R1 (Figure 3c), however, above 200μM Mn, control HEK cells had an attenuated response to Mn. The curve could be described by Michaelis-Menton kinetics for a saturable system, wherein absorption rates slow as internal concentration of Mn rises. In contrast, the increase in R1 with [Mn] in *+MntR** cells was linear at these concentrations (R^2=0.997), suggesting an increased capacity to store Mn before saturation occurs.

MntR* retains Mn in cells, and acts synergistically with DMT1

Based on the data suggesting that MntR improves Mn retention in cells, we moved from HEK cells into a model previously demonstrated to have poor Mn retention both in vitro and in vivo (6). Specifically, B16 melanoma cells lose their R1 gains very quickly after Mn supplementation (Figure 4) (6), and therefore provided an excellent model to test MntR. Stable cell lines were generated from B16 cells (*+MntR**) and from B16 cells which already overexpressed DMT1 (*+D+M*). There was no significant difference in MntR expression between the two constructs (p=0.14, n=8).

Control B16 cells demonstrated a less distinct Mn saturation curve compared to HEK cells (Figure 4a, 3c). DMT1-expressing B16 cells (*+DMT1*) gave consistently higher R1 values, though the saturation effect was still apparent. R1 values for supplemented B16 and *+DMT1* cells were similar to previously reported values, with a maximal R1 shift of 55% (Figure 4a) (6). Compared to the control HEK cells, *+MntR** cells again yielded a linear response to Mn supplementation resulting in a large increase in R1 at high supplementations with a maximal 38% gain, approaching *+DMT1* gains. *+D+M* cells gave the largest increase in R1, with overall R1 gains greater than the sum of each components effect (Figure 4a). At the lowest level of supplementation (100μM), the R1 values for the *+D+M* cells was greater than that for either *+DMT1* or *+MntR** alone at 300μM. This resulted in a 166% gain in R1 at 100μM and 96% at 300μM, comparing *+D+M* to control B16 cells. This enhancement was far greater than the cumulative effect of either DMT1 or MntR* alone and suggests that improving both Mn uptake (DMT1) and retention (MntR*) can act synergistically to enhance R1 in the cell. At the highest levels of supplementation however, dual expression of DMT1 and MntR* was only cumulative at best. Comparing the saturation curves, both the *+DMT1* and *+D+M* cell lines are nearing saturation at 300μM Mn, suggesting diminishing returns at high levels of supplementation.

The advantages of MntR* became more apparent after Mn had been washed from the B16 cells. In a time course study cells were supplemented with 300μM Mn then washed and incubated in fresh, unsupplemented, media for up to 48h (Figure 4b). Control B16 cells and *+DMT1* cells lost almost all of their Mn based R1 improvements within 2 hours of

supplementation, similar to previous reported data (6). For both +*MntR** and +*D*+*M* B16 cells, the post Mn washout kinetics were more complex. These cell lines did not begin to lose their R1 gains for 2 hours after removal of Mn, and retained a significantly higher R1 than control cell lines up to 24 hours after supplementation, showing a 96% improvement in R1 at 12h post supplementation. +*D*+*M* lines again gave a synergistic effect showing significant improvements in R1 up to 48h after supplementation with 216% R1 gains at 12h. Both +*MntR** and the +*D*+*M* lines gave a similar R1 profile overall with a bimodal release of Mn over time.

MntR* creates in vivo contrast in a tumor model

B16 melanoma cells are tumorigenic in C57Bl/6 mice, making a ready transition from in vitro cell characterization to in vivo expression of MntR*. We chose this cell line based on previous work with DMT1, wherein it was the weakest example of in vivo contrast with a very narrow window after Mn-supplementation in which contrast was significant (6). Based on the in vitro cell results described above, the expression of MntR* could potentially produce lasting contrast in vivo where DMT1 could not. In our cell based assays we examined dual DMT1 and MntR* expression in double transfected stable expressing cells. This would be an impractical strategy for in vivo expression, therefore we made a single multicistronic construct which expressed DMT1, MntR* and eGFP, which could be readily employed for future in vivo studies, to generate additional +D+M B16 cell lines. We then conducted a longitudinal comparison of control, +MntR* and +D+M B16 melanoma tumors, using a dual flank tumor model imaged with MEMRI.

Both +*MntR** and +*D*+*M* tumors were brighter than control B16 tumors and adjacent normal tissues in T1-weighted images acquired 3h after Mn administration (Figure 5a,b), similar to +*DMT1* B16 tumors reported previously (6). Unlike the previous measurements in +*DMT1* B16 tumors (6), both +*MntR** and +*D*+*M* tumors retained significant and visually obvious contrast at 6h post Mn administration, compared to control B16 tumors (Figure 5a–c; *$p<0.01$, n=5 for each comparison). At the 6h time-point, dual expression of DMT1 and MntR* in the +*D*+*M* tumors retained slightly higher contrast, compared to +*MntR** tumors, though the difference was not statistically significant ($p=0.1$, n=5). These results were largely consistent with the in vitro experiments, demonstrating that MntR can potentially function better as a reporter than DMT1 after Mn administration in some cell types. The similar in vivo results for the +*MntR** and the +*D*+*M* B16 tumors likely shows how Mn pharmacokinetics may favor engineered retention over uptake for some cell types.

DISCUSSION

The results of this study demonstrate that MntR has potential for application as an MRI reporter protein, but only when expressed within the GA, the sub-cellular organelle where Mn is concentrated. MntR was chosen as a candidate reporter based on its high affinity to Mn and its atomic structure, in which the Mn-binding motif leaves Mn exposed to interact with the spin lattice (19), a requirement for any T1-agent. However, MntR binds Mn reversibly, taking shape only when enough ambient Mn is present (21), and making sub-cellular localization of MntR critical for reporter function. This increases the complexity of

design of Mn and other paramagnetic metal-binding proteins as expressible MRI contrast agents, making it imperative to understand not only their chelation properties, but also the underlying biology of metal transport, storage and release within the expressing cells.

Our initial results clearly showed the capacity of MntR as a Mn chelator, but significant additional engineering was required to demonstrate utility as an expressible contrast agent for MRI. Specifically, MntR* was optimized for expression in mammalian cells, and targeted to the cis-Golgi, the region of the GA adjacent to the ER where Mn is most enriched. The data suggests MntR* augments the endogenous biology to hold Mn in the cell longer than normal, but not indefinitely. This is best described by mass action kinetics where, in the cell, Mn should exist partly as free ionic Mn and partly bound to proteins at a wide range of affinities. Expression of MntR* expands the buffered pool of Mn thereby increasing the overall Mn. By this model, MntR* expression would only increase the saturation point of Mn without changing the rates of uptake and release of free Mn. This can be seen in the concentration curves for both HEK and B16 cells, where the control and +MntR* curves differ only as control cells reach saturation (Fig 3a,4a). At the lowest levels of Mn supplementation, there should be no difference in the slope of control vs +*MntR** cells, unlike DMT1 expression, which, by altering the rate of uptake, should increase the initial slope of the line without changing the shape of the curve (Fig 4a).

Notably, the T1/R1 changes during Mn washout in B16 melanoma cells expressing MntR* showed two modes of Mn release, one occurring on a fast time-scale within 5 hours, and the other more slowly. The loss rate of free Mn should not be effected by MntR*, and the pool of Mn that is free at equilibrium may leave the cells on the order of seconds to minutes, meaning the release profile is almost entirely from the pool of buffered Mn. There are two likely reasons for a bimodal Mn release profile. At the molecular level, MntR has two binding sites with different affinities for Mn, 0.2–2μM for the first site and 5–13μM at the second (33). The release profile could be due to the two rates of disassociation as Mn is cleared from each binding site, but this would require high cooperativity between the two sites, a property that has not been confirmed. A more likely possibility is that the data shows two modes of egress from the cell. We propose that Mn can exit the Golgi and the cell via known Ca transport mechanisms, directly through the cytosol and, much more slowly, via the secretory pathway. Given the low selectivity of many Ca transport mechanisms this seems likely, however their permissivity to Mn has not been shown to date.

Our results also indicate that DMT1 and MntR* can be used in combination, to enhance cell uptake and retention of Mn, respectively. These results were most obvious in cultured cells, in vitro. In vivo, the combined expression of DMT1 and MntR* showed a similar trend, but the results did not achieve statistical significance. This highlights the challenges of developing reporter systems for in vivo applications: a tumor within a living animal is very different from the same tumor cells in culture, and optimizations done in vitro may not translate in vivo. This is not surprising since the B16 cells were chosen specifically because of their enhanced ability to excrete Mn, compared to other cells tested (6). The rate of Mn delivery to the cells as Mn moves through the vasculature and interstitial space, as well as the gradual reduction of Mn, present a challenge to any sort of kinetic model. We conclude from these results that retention of Mn is potentially as important as Mn uptake for a Mn-

based MRI reporter, but the optimal combination of the two can only be determined as more in vivo models are explored with these technologies.

Beyond the goal of creating genetic reporters for MEMRI, the process of engineering MntR into a functional contrast agent has provided key insights into cellular Mn biology and what the contrast created in MEMRI actually shows. Mn is not simply a cellular marker in MEMRI, it is actually functioning, at least in some situations, as a Golgi stain or marker of the secretory pathway. This view greatly illuminates existing studies using MRI tract tracing with Mn, which depends on the Mn traveling anteriogradely along axonal pathways (4,5). While the MEMRI community generally accepts that Mn transport is an active process, the data presented here supports a model wherein the movement of Mn along axons is specifically transported via components of the Golgi and Golgi-associated vesicles. This is a critical concept as MEMRI moves into reporter gene imaging. Cell types such as Purkinje and granule cells in the cerebellum, or pyramidal neurons in the cortex have distinct layers where their cell bodies are located with extended axons and dendrites forming separate layers (34). MEMRI signal in these cell types could therefore be found peripheral to the cell bodies within the layers innervated by the axons and dendrites.

MntR and DMT1 represent the first elements of an expanding tool set that can be expressed alone or in combination to maximize Mn-based MRI contrast. The current construct, resulting in DMT1/MntR* co-expression can already be integrated into most viral and transgenic expression systems currently in use. Further refinements such as minimization of the Cab45 targeting component to MntR*, and/or optimization of DMT1/MntR* expression ratios, will be important for implementation with larger promoters in expression constructs. Advances in these areas could make possible dynamic studies of in vivo gene expression, longitudinal cell fate mapping using Cre or other site specific recombinases (35), or activity dependent neuronal circuit mapping, for example using using cfos-tTA transgenic approaches (36). MEMRI has already become an increasingly important method for small animal imaging and with technologies to engineer the uptake and retention of Mn, genetic imaging studies with MEMRI have become a feasible method for exploring biological questions in vivo.

ACKNOWLEDGMENTS

This research was supported by NIH grant R01NS038461. MRI imaging was partially supported by the Small Animal Imaging Core at NYU School of Medicine, and the NYU Cancer Institute through the Cancer Center Support Grant (P30CA016087). We thank Dr. John Helmann (Cornell) for providing the bacterial MntR in a pET17b expression vector. We also thank the following people for their contributions: Andrea Gomez for her advice and assistance with cell culture, Kerryanne Winters for management of cell lines, Daniel Colon for maintaining mice used in these experiments, Victor Lelyveld (MIT) for discussions of the data analysis, and Professor Alan Jasanoff (MIT) for his patience and insights on Mn kinetics. Some of the authors also thank Todd Polenberg and Sarah Porter for logistical support during the final phases of the work.

REFERENCES

1. Massaad CA, Pautler RG. Manganese-Enhanced Magnetic Resonance Imaging (MEMRI). Methods Mol. Biol. 2011; 711:145–174. [PubMed: 21279601]
2. Lin YJ, Koretsky AP. Manganese Ion Enhances T1-Weighted MRI during Brain Activation: An Approach to Direct Imaging of Brain Function. Magn Reson Med. 1997; 38:378–388. [PubMed: 9339438]

3. Yu X, Wadghiri YZ, Sanes DH, Turnbull DH. In Vivo Auditory Brain Mapping in Mice with Mn-Enhanced MRI. Nat. Neurosci. 2005; 8:961–968. [PubMed: 15924136]
4. Pautler RG, Silva AC, Koretsky AP. In Vivo Neuronal Tract Tracing Using Manganese-Enhanced Magnetic Resonance Imaging. Magn Reson Med. 1998; 40:740–748. [PubMed: 9797158]
5. Pautler RG, Mongeau R, Jacobs RE. In Vivo Trans-Synaptic Tract Tracing from the Murine Striatum and Amygdala Utilizing Manganese Enhanced MRI (MEMRI). Magn Reson Med. 2003; 50:33–39. [PubMed: 12815676]
6. Bartelle BB, Szulc KU, Suero-Abreu GA, Rodriguez JJ, Turnbull DH. Divalent Metal Transporter, DMT1: A Novel MRI Reporter Protein. Magn Reson Med. 2012
7. Picard V, Govoni G, Jabado N, Gros P. Nramp 2 (DCT1/DMT1) Expressed at the Plasma Membrane Transports Iron and Other Divalent Cations into a Calcein-Accessible Cytoplasmic Pool. J. Biol. Chem. 2000; 275:35738–35745. [PubMed: 10942769]
8. Dürr G, Strayle J, Plemper R, Elbs S, Klee SK, Catty P, Wolf DH, Rudolph HK. The Medial-Golgi Ion Pump Pmr1 Supplies the Yeast Secretory Pathway with Ca2+ and Mn2+ Required for Glycosylation, Sorting, and Endoplasmic Reticulum-Associated Protein Degradation. Mol. Biol. Cell. 1998; 9:1149–1162. [PubMed: 9571246]
9. Mukhopadhyay S, Linstedt AD. Identification of a Gain-of-Function Mutation in a Golgi P-Type ATPase That Enhances Mn2+ Efflux and Protects against Toxicity. Proc Natl Acad Sci U S A. 2011; 108:858–863. [PubMed: 21187401]
10. Krause, W. Contrast Agents I: Magnetic Resonance Imaging. Berlin: Springer; 2002. p. 249
11. Major JL, Meade TJ. Bioresponsive, Cell-Penetrating, and Multimeric MR Contrast Agents. Acc. Chem. Res. 2009; 42:893–903. [PubMed: 19537782]
12. Strauch RC, Mastarone DJ, Sukerkar PA, Song Y, Ipsaro JJ, Meade TJ. Reporter Protein-Targeted Probes for Magnetic Resonance Imaging. Journal of the American Chemical Society. 2011
13. Ilies M, Di Costanzo L, North ML, Scott JA, Christianson DW. 2-Aminoimidazole Amino Acids as Inhibitors of the Binuclear Manganese Metalloenzyme Human Arginase I. J. Med. Chem. 2010; 53:4266–4276. [PubMed: 20441173]
14. Vyas NK, Nickitenko A, Rastogi VK, Shah SS, Quiocho FA. Structural Insights into the Dual Activities of the Nerve Agent Degrading Organophosphate Anhydrolase/prolidase. Biochemistry. 2010; 49:547–559. [PubMed: 20000741]
15. Guan Y, Hickey MJ, Borgstahl GE, Hallewell RA, Lepock JR, O'Connor D, Hsieh Y, Nick HS, Silverman DN, Tainer JA. Crystal Structure of Y34F Mutant Human Mitochondrial Manganese Superoxide Dismutase and the Functional Role of Tyrosine 34. Biochemistry. 1998; 37:4722–4730. [PubMed: 9537987]
16. Zhang Y, Deshpande A, Xie Z, Natesh R, Acharya KR, Brew K. Roles of Active Site Tryptophans in Substrate Binding and Catalysis by Alpha-1,3 Galactosyltransferase. Glycobiology. 2004; 14:1295–1302. [PubMed: 15229192]
17. Ramakrishnan B, Ramasamy V, Qasba PK. Structural Snapshots of Beta-1,4-Galactosyltransferase-I along the Kinetic Pathway. J. Mol. Biol. 2006; 357:1619–1633. [PubMed: 16497331]
18. Glasfeld A, Guedon E, Helmann JD, Brennan RG. Structure of the Manganese-Bound Manganese Transport Regulator of Bacillus Subtilis. Nat. Struct. Biol. 2003; 10:652–657. [PubMed: 12847518]
19. Golynskiy MV, Davis TC, Helmann JD, Cohen SM. Metal-Induced Structural Organization and Stabilization of the Metalloregulatory Protein MntR. Biochemistry. 2005; 44:3380–3389. [PubMed: 15736948]
20. Patzer SI, Hantke K. Dual Repression by Fe(2+)-Fur and Mn(2+)-MntR of the mntH Gene, Encoding an NRAMP-like Mn(2+) Transporter in Escherichia Coli. J. Bacteriol. 2001; 183:4806–4813. [PubMed: 11466284]
21. Waters LS, Sandoval M, Storz G. The Escherichia Coli MntR Mini Regulon Includes Genes Encoding a Small Protein and an Efflux Pump Required for Manganese Homeostasis. J Bacteriol. 2011

22. Gruppi F, Liang J, Bartelle BB, Royzen M, Turnbull DH, Canary JW. Supramolecular Metal Displacement Allows on-Fluorescence Analysis of manganese(II) in Living Cells. Chem. Commun. (Camb.). 2012; 48:10778–10780. [PubMed: 23023093]

23. Morello M, Canini A, Mattioli P, Sorge RP, Alimonti A, Bocca B, Forte G, Martorana A, Bernardi G, Sancesario G. Sub-Cellular Localization of Manganese in the Basal Ganglia of Normal and Manganese-Treated Rats: An Electron Spectroscopy Imaging and Electron Energy-Loss Spectroscopy Study. NeuroToxicology. 2008; 29:60–72. [PubMed: 17936361]

24. Da Costa AG, Madeira VMC. Magnesium and Manganese Ions Modulate Ca2+ Uptake and Its Energetic Coupling in Sarcoplasmic Reticulum. Archives of Biochemistry and Biophysics. 1986; 249:199–206. [PubMed: 2943223]

25. Carmona A, Devès G, Roudeau S, Cloetens P, Bohic S, Ortega R. Manganese Accumulates within Golgi Apparatus in Dopaminergic Cells as Revealed by Synchrotron X-Ray Fluorescence Nanoimaging. ACS Chemical Neuroscience. 2010; 1:194–203. [PubMed: 22778823]

26. Rivinoja A, Hassinen A, Kokkonen N, Kauppila A, Kellokumpu S. Elevated Golgi pH Impairs Terminal N-Glycosylation by Inducing Mislocalization of Golgi Glycosyltransferases. J. Cell. Physiol. 2009; 220:144–154. [PubMed: 19277980]

27. Dode L, Andersen JP, Raeymaekers L, Missiaen L, Vilsen B, Wuytack F. Functional Comparison between Secretory Pathway Ca2+/Mn2+-ATPase (SPCA) 1 and Sarcoplasmic Reticulum Ca2+-ATPase (SERCA) 1 Isoforms by Steady-State and Transient Kinetic Analyses. J. Biol. Chem. 2005; 280:39124–39134. [PubMed: 16192278]

28. Szymczak-Workman AL, Vignali KM, Vignali DAA. Design and Construction of 2A Peptide-Linked Multicistronic Vectors. Cold Spring Harb Protoc. 2012; 2012:199–204. [PubMed: 22301656]

29. Haas IG. BiP (GRP78), an Essential hsp70 Resident Protein in the Endoplasmic Reticulum. Experientia. 1994; 50:1012–1020. [PubMed: 7988659]

30. Zhang Y, Kang Y-H, Chang N, Lam PPL, Liu Y, Olkkonen VM, Gaisano HY. Cab45b, a Munc18b-Interacting Partner, Regulates Exocytosis in Pancreatic Beta-Cells. J. Biol. Chem. 2009; 284:20840–20847. [PubMed: 19487699]

31. Teasdale RD, Jackson MR. Signal-Mediated Sorting of Membrane Proteins between the Endoplasmic Reticulum and the Golgi Apparatus. Annu. Rev. Cell Dev. Biol. 1996; 12:27–54. [PubMed: 8970721]

32. Wadghiri YZ, Blind JA, Duan X, Moreno C, Yu X, Joyner AL, Turnbull DH. Manganese-Enhanced Magnetic Resonance Imaging (MEMRI) of Mouse Brain Development. NMR Biomed. 2004; 17:613–619. [PubMed: 15761950]

33. Kliegman JI, Griner SL, Helmann JD, Brennan RG, Glasfeld A. Structural Basis for the Metal-Selective Activation of the Manganese Transport Regulator of Bacillus Subtilis. Biochemistry. 2006; 45:3493–3505. [PubMed: 16533030]

34. Kandel, E.; Schwartz, J.; Jessell, T. Principles of Neural Science, Fifth Edition. McGraw Hill Professional; 2013. p. 1761

35. Legué E, Joyner AL. Genetic Fate Mapping Using Site-Specific Recombinases. Meth. Enzymol. 2010; 477:153–181. [PubMed: 20699142]

36. Reijmers L, Mayford M. Genetic Control of Active Neural Circuits. Front Mol Neurosci. 2009; 2

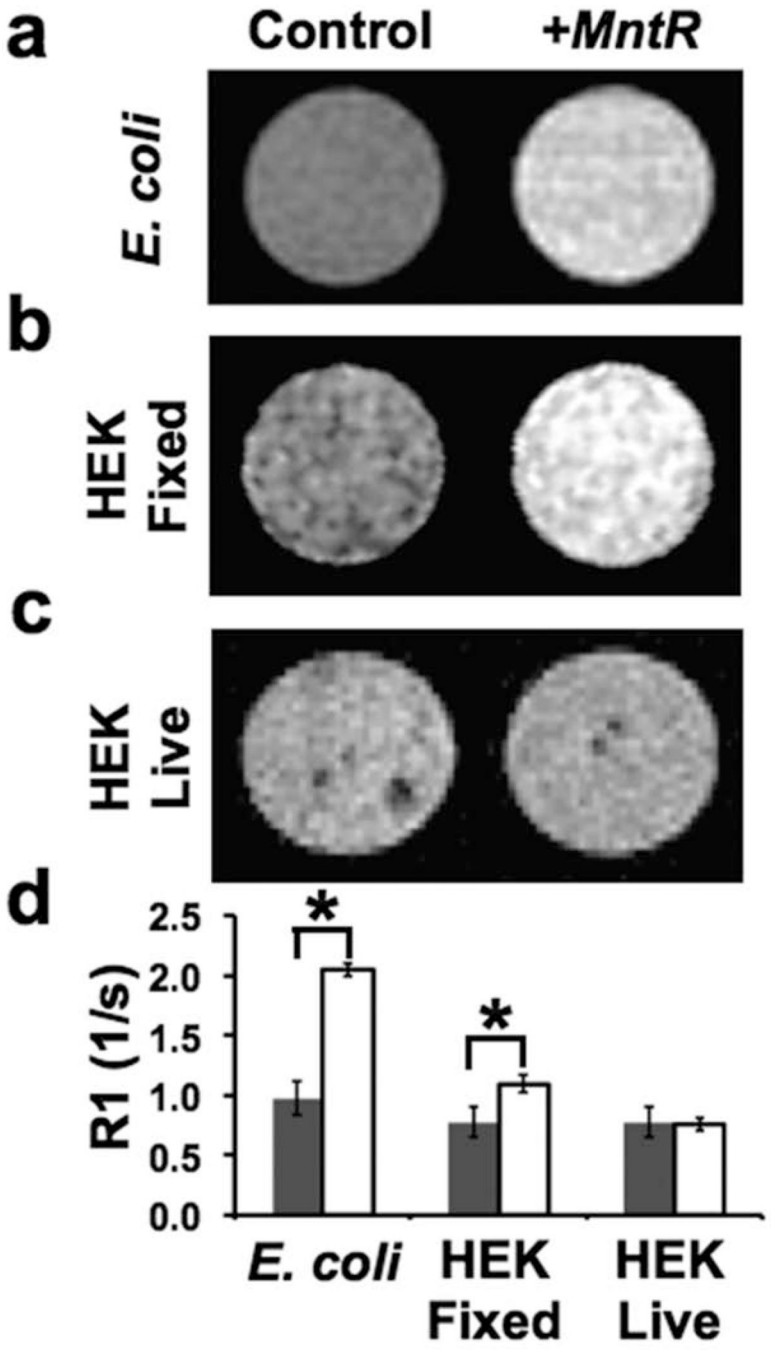

Figure 1. MntR was expressed in bacterial and mammalian cells

(**a**) B21 bacterial (*E. coli*) cells were transformed with inducible MntR. Inducing expression of MntR (+*MntR*) resulted in T1 contrast under standard culture conditions. (**b**) In HEK cells expressing MntR (+*MntR*), contrast was visually obvious compared to control when cells were fixed and scanned ex vivo. (**c**) In living HEK cells, T1 contrast was indistinguishable from control cells. (**d**) R1 relaxometry showed a significant R1 difference (+*MntR* vs control) in bacteria (n=4 for each group) and fixed HEK cells (*p<0.001; n=6 +*MntR*, n=4

control), but no significant difference in the live HEK cells (p=0.6; n=6 +*MntR*, n=4 control).

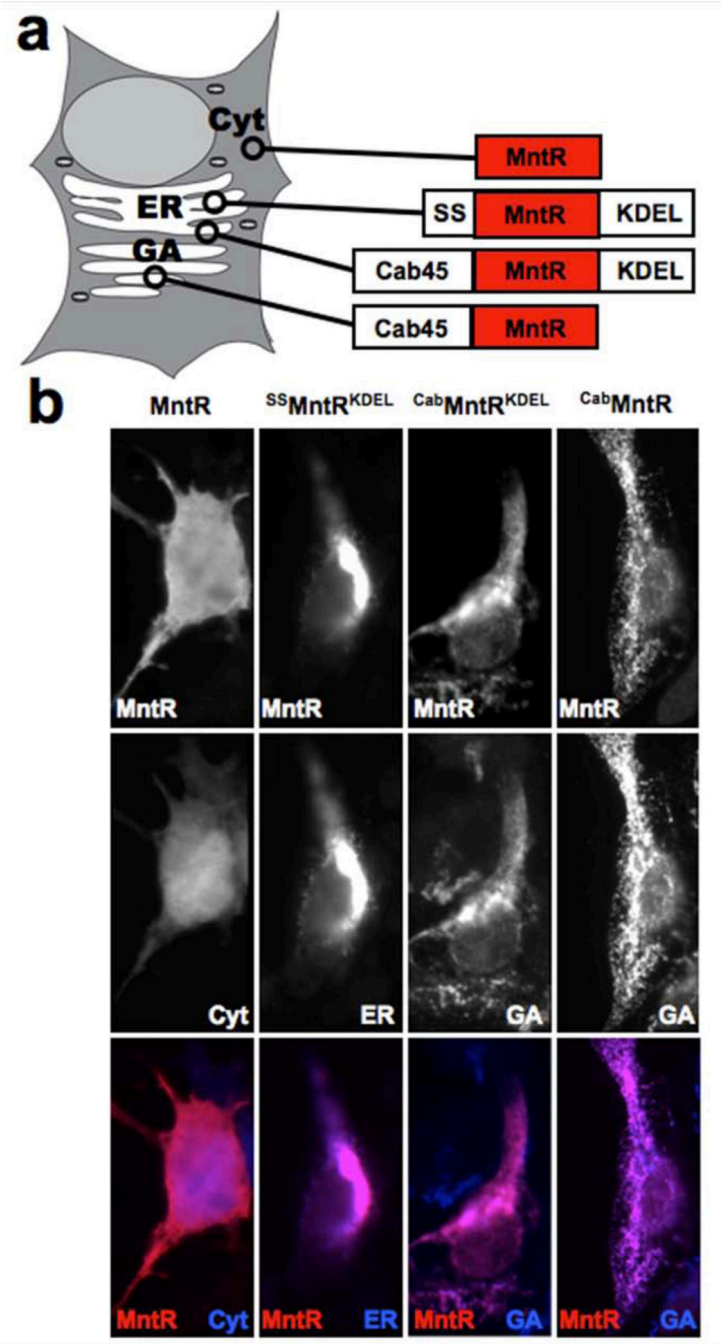

Figure 2. Engineering subcellular localization of MntR

(**a**) The schematic shows the different MntR localization tags and subcellular locations being targeted. The tags employed included an N-terminal signal sequence (SS) for entry into the secretory pathway, a C-terminal amino acid KDEL sequence for retention in the Endoplasmic Reticulum (ER), and a fusion of MntR with Cab45 for localization within the Golgi Apparatus (GA). (**b**) Immunohistochemistry was performed on HEK cells expressing the MntR localization chimeras, co-stained with subcellular markers. Without engineering MntR expressed in the cytosol, similar to GFP. With the addition of the SS and KDEL

sequences, MntR entered the secretory pathway and was localized in the ER. Fusion with Cab45 also brought MntR into the secretory pathway, but was localized more distally, in the GA. The ^{Cab}MntR fusion localization was indistinguishable from ^{Cab}MntR^{KDEL} by immunostaining, since both colocalized with the GA marker.

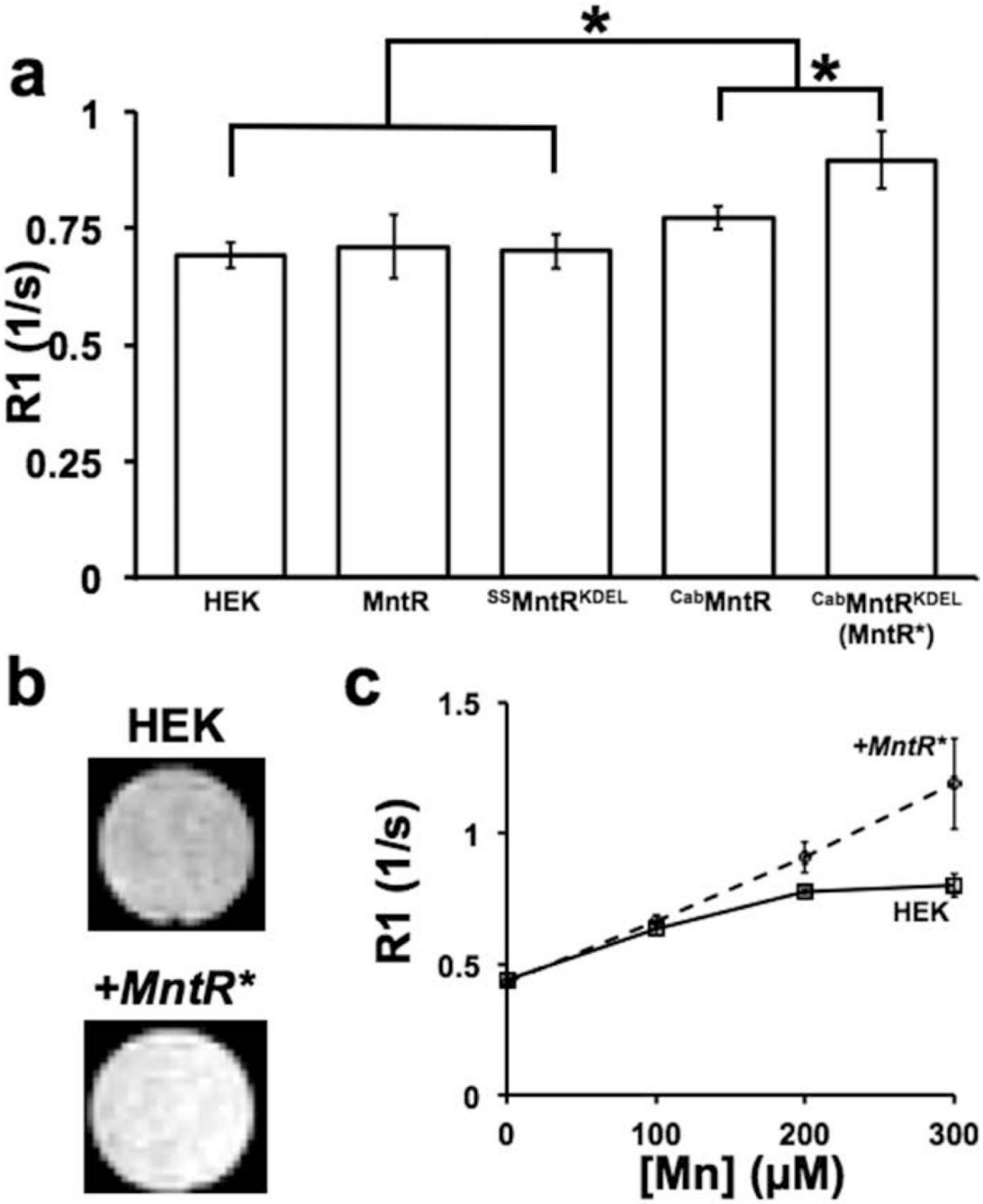

Figure 3. Golgi localized MntR increased R1 in live HEK cells

(**a**) R1 was measured in HEK cells transiently transfected with each MntR localization chimera and supplemented with 300uM Mn. ^{Cab45}MntR significantly increased R1 compared to untransfected HEK cells and HEK cells expressing nontargeted MntR and ER-targeted ^{SS}MntR^{KDEL} (*p<0.001, n = 6–10 for each group). ^{Cab45}MntR^{KDEL} (MntR*) showed further significant improvements over the single fusion ^{Cab45}MntR chimera. (**b**) R1 changes between untransfected and MntR*-expressing (+*MntR**) HEK cells resulted in visually obvious contrast in T1 weighted images. (**c**) R1 was measured at varying Mn

concentrations to compare control HEK cells and a stable +*MntR** cell line. The +*MntR** cells showed a more linear increase in R1 up to 300μM compared to control HEK cells, resulting in increased contrast at higher concentrations of Mn (n 4 for each trial).

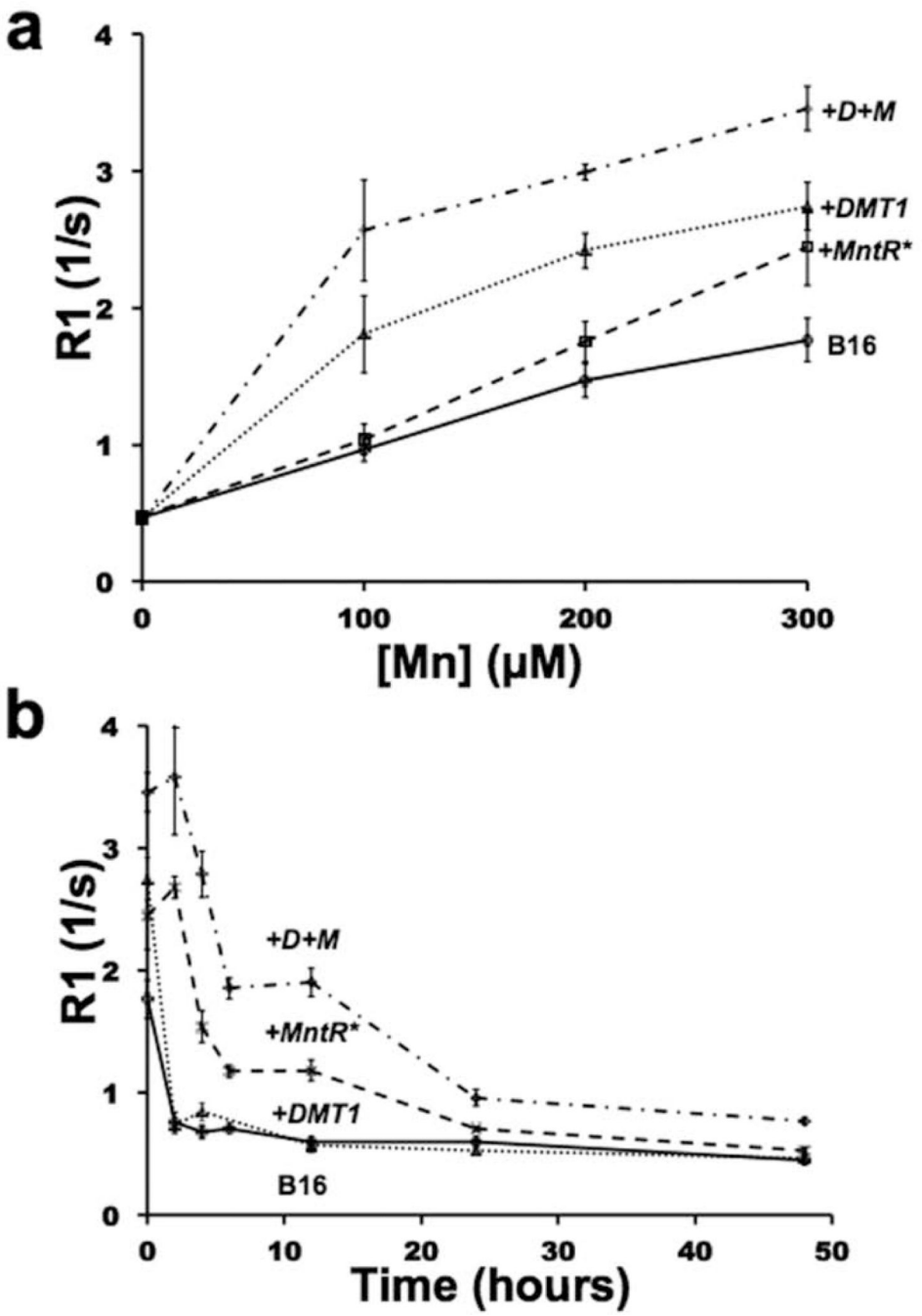

Figure 4. MntR* retained contrast over time and worked synergistically with DMT1 in B16 melanoma cells

(**a**) R1 was measured as a function of Mn-supplementation in control B16 cells and in stable B16 cell lines expressing MntR* (+*MntR**), DMT1 (+*DMT1*), as well as cells expressing both proteins (+*D*+*M*). (**b**) Time course R1 data was also analyzed in each cell line after supplementation for 1h with 300μM Mn, then washed and cultured in control media for up to 48 h. Maximal gains in R1 are apparent in the ***+D+M*** cells (n 4 trials for each data point).

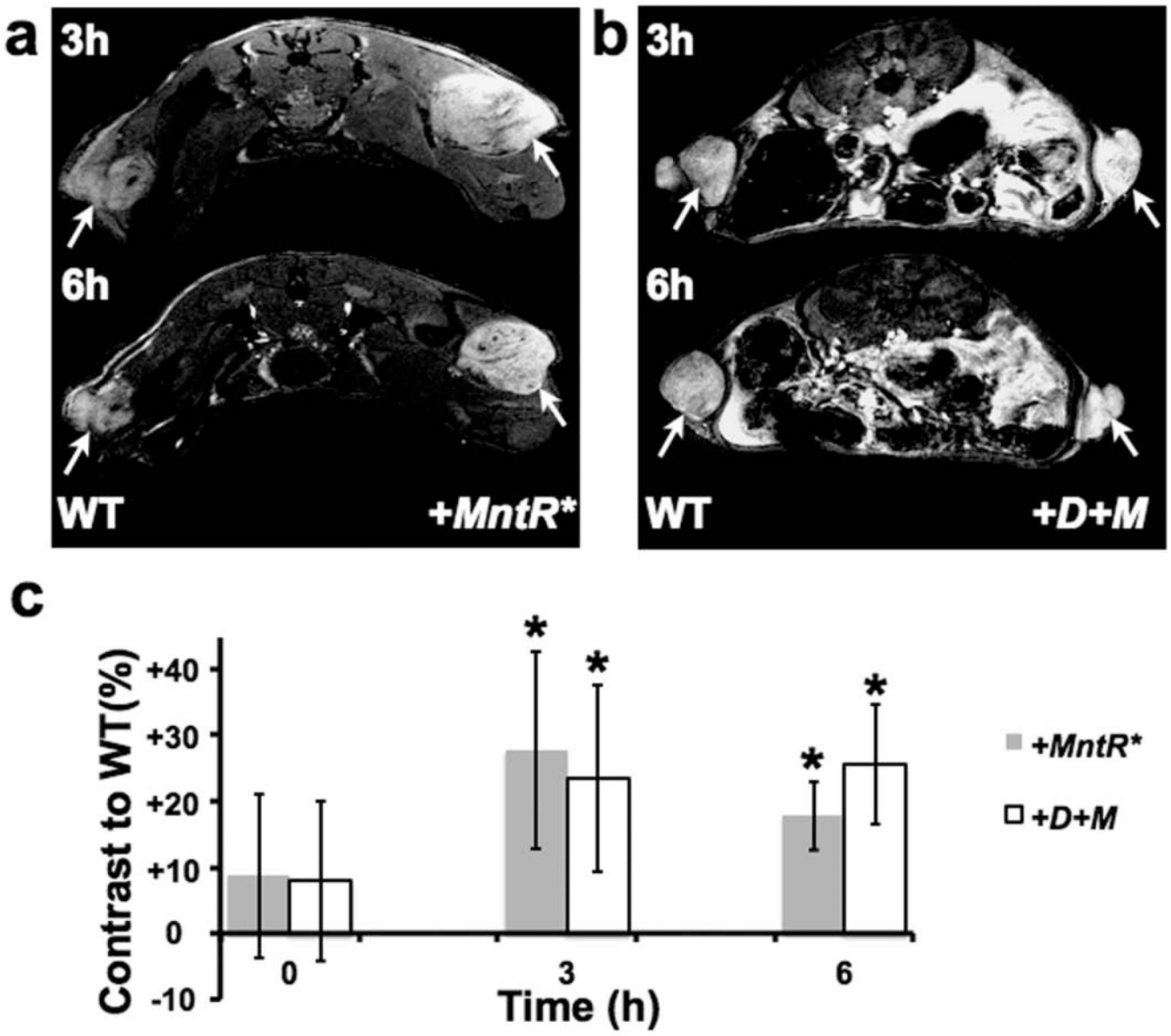

Figure 5. MntR* expression and dual expression of DMT1 and MntR* allow for extended contrast in a B16 melanoma model

(**a**) In a dual tumor model using control and MntR*-expressing (+*MntR**) B16 cells, +*MntR** tumors produced visually obvious contrast over control B16 cells at 3 and 6 hours (tumors marked by white arrows). (**b**) Similarly, dual expression of DMT1 and MntR* (+*D*+*M*) showed obvious contrast compared to controls at both time points. (**c**) In time course experiments, contrast measured in +*MntR** and +*D*+*M* tumors, compared to B16 controls (n=5 mice for each tumor type), showed persistent and significant positive increases in signal intensity, creating up to 25% contrast in vivo. (See text for the results of the statistical analyses).